Medicinal Chemistry Research (2022) 31:1594–1610
https://doi.org/10.1007/s00044-022-02935-6

MEDICINAL CHEMISTRY RESEARCH

ORIGINAL RESEARCH

Synthesis, characterization, and biological evaluation of some novel ϒ-aminobutyric acid aminotransferase (GABA-AT) inhibitors

Sushant Kumar Shrivastava[1] · Ojaswi Sinha[1] · Munish Kumar[1] · Digambar Kumar Waiker[1] · Akash Verma[1] · Prabhash Nath Tripathi[1,2] · Bhagwati Bhardwaj[1] · Poorvi Saraf[1]

Received: 29 April 2022 / Accepted: 8 July 2022 / Published online: 29 July 2022

Abstract

In our present work, some novel substituted 4-phenyl-5-vinylpyrrolidin-2-one derivatives were designed, synthesized, and evaluated for their γ-aminobutyric acid-aminotransferase (GABA-AT) inhibition and in-vivo anticonvulsant activity. Among all the synthesized derivatives, compound **7f** was observed as the most potent and competitive inhibitor of GABA-AT ($IC_{50} = 46.29 \pm 3.19$ μM, $K_i = 0.106 \pm 0.004$ μM). The in-vivo anticonvulsant activity against maximum electroshock (MES) and PTZ, induced seizures test of compound **7f**, was observed very significantly ($P < 0.05$) in comparison with standard Vigabatrin and have shown an increase in the level of GABA in the cortex region of the brain. The ex-vivo studies have also suggested reduced tissue necrosis. Finally, In-silico molecular docking and dynamics studies of compound **7f** have shown that it forms desired amino acid residue interactions with the GABA-AT and was stable for 50 ns in the active site pocket of the enzyme.

Keywords Epilepsy · Anti-Epileptic Drugs · GABA-AT Inhibitors · Vigabatrin

Abbreviations

GABA	γ-aminobutyric acid
EDC	1-Ethyl-3-(-3-dimethyl aminopropyl) carbodiimide
HOBt	1-hydroxy-benzotriazole
Ki	inhibition constant
SGF	Simulated gastric fluid
SIF	Simulated intestinal fluid
HLTE	Hind Limb Tonic Extensor
TEBA	benzyltriethylammonium chloride.

Introduction

γ-Amino Butyric Acid (GABA) is the most important inhibitory neurotransmitter in the cerebral cortex region of the brain that counterbalances the neuronal excitation and controls various neuropsychiatric activities in the brain [1, 2]. GABA-AT (γ-aminobutyric acid aminotransferase) is a pyridoxal 5′-phosphate-(PLP) dependent enzyme that is responsible for GABA, which leads to numerous GABA-AT related CNS disorders [3].

GABA is generated and stored in synaptic vesicles in neurons, and it is released from these vesicles to the synapse, where it plays a crucial role in brain signaling [4]. The optimum GABA concentration in the synapse is necessary to control the firing of the neurons. The concentration of GABA below a threshold level results in behavioral and functional changes such as epilepsy, seizures, Alzheimer's disease, Parkinson's disease, etc. [5–8]. The GABA, an inhibitory neurotransmitter along with L-glutamate (excitatory neurotransmitter), regulates the neuronal activity in the brain. The concentration of GABA in the brain is governed by enzymes, namely (PLP) dependent enzyme and glutamic acid decarboxylase that together convert L-glutamate to GABA [9]. Many studies suggest that inhibition of GABA-AT causes an increased GABA concentration in the brain and may reduce or

Supplementary information The online version contains supplementary material available at https://doi.org/10.1007/s00044-022-02935-6.

✉ Sushant Kumar Shrivastava
skshrivastava.phe@itbhu.ac.in

[1] Pharmaceutical Chemistry Research Laboratory, Department of Pharmaceutical Engineering and Technology, Indian Institute of Technology (Banaras Hindu University), Varanasi 221005 U.P., India

[2] Department of Pharmaceutical Technology, Meerut Institute of Engineering and Technology, Meerut 25000 U.P., India

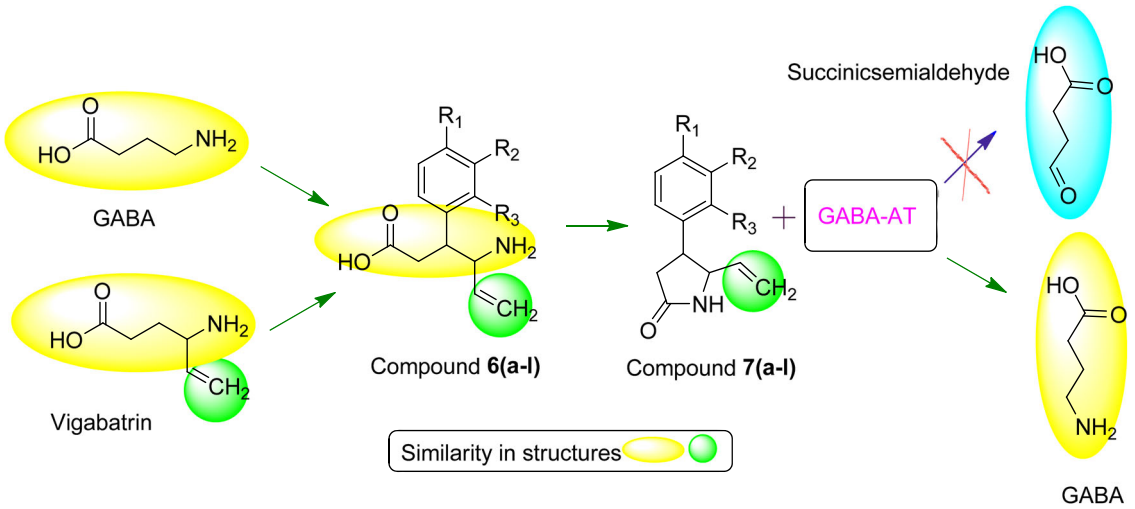

Fig. 1 The designing strategy of the compounds **7(a-l)**

suppress the impaired neuropsychiatric conditions that occurred due to its lower threshold level.

Various GABA-AT inhibitors have been reported in the last few years, and among them, Vigabatrin is the most potent, highly selective, and FDA-approved irreversible inhibitor of the GABA-AT and does not affect the other enzymatic pathway of GABA [10], though, it has limited direct application over GABA therapy due to its serious adverse effects such as gastrointestinal tract (GIT) disturbance and neuropathy [11]. A higher dose of Vigabatrin is also required to cross BBB (blood-brain barrier) due to its higher water solubility and thus reduces its efficacy. Apart from Vigabatrin, few other molecules are also reported against GABA-AT with improved efficacy (in-vivo models) and few are also under clinical trials. Therefore, it is an important need to develop a small molecule, an inactivator of GABA-AT as an alternative to Vigabatrin.

The design consideration includes the development of small molecules that can bind irreversibly with the GABA-AT receptor and could also cross the blood-brain barrier with considerable efficacy. Considering all possible structural requirements necessary for a small molecule to become a potent GABA-AT inhibitor, a series of substituted 4-phenyl-5-vinylpyrrolidin-2-one derivatives has been designed and synthesized. The first aim of our work was to enhance the lipophilicity of the molecule greater than that of the Vigabatrin and the second aim was to keep the GABA-AT inhibitory effect similar to that of Vigabatrin. The presence of amino and carboxylic acid terminals of GABA residue is believed to produce GIT disturbances at gastric pH. To suppress the above mention problem, we tried to cyclize amino and carboxylic acid terminal of the GABA residue into substituted pyrrolidine-2-one derivatives **7(a–l)**. In our work, we have designed a series with few assumptions, such as a substituted aromatic ring at 4-position of pyrrolidin-2-one scaffold will show π-π interaction with the enzyme amino acid residues thus predicted to increase its lipophilicity, a vinyl group (also present in Vigabatrin) present in the structure of the designed nucleus will impart its selectivity toward GABA-AT as it binds with the accessory binding pocket present in the enzyme. The designed molecule with all the possible interactions with the active site is believed to bind irreversibly with the GABA-AT and is also expected to increase GABA concentration in the brain (Fig. 1).

Result and discussion

Chemistry

The imine derivative are synthesized in the first step by reacting allylamine with benzaldehyde via nucleophillic addition reaction to get Phenyl methylidene-prop-2-en-1-yl amine (**3**) (Scheme 1). The imine derivative acts as Michael donor group and undergoes Michael's addition reaction with cinnamic acid derivatives **4(a–l)** with the formation of carbon-carbon bond and results in 3-phenyl-4(phenyl methylidene amino) hex-5-enoic acid **5(a–l)** (Table 1) [12]. Further, the imine bond was hydrolyzed to form a 4-amino-3-phenyl hex-5-enoic acid **6(a–l)** [13]. The hydrolyzed products **6(a–l)** were subjected to EDC and HOBt, which are used as carboxyl group activating agents to yield amide bonds by the coupling of primary amines and resulted in substituted pyrrolidine-2-one derivatives **7(a–l)**. The completion of the reaction was monitored by the TLC, and the synthesized compound was purified by crystallization.

^{1}H NMR spectral analysis

^{1}H NMR spectra of intermediate (**3**) were confirmed by the presence of aromatic protons, the disappearance of (-NH_2)

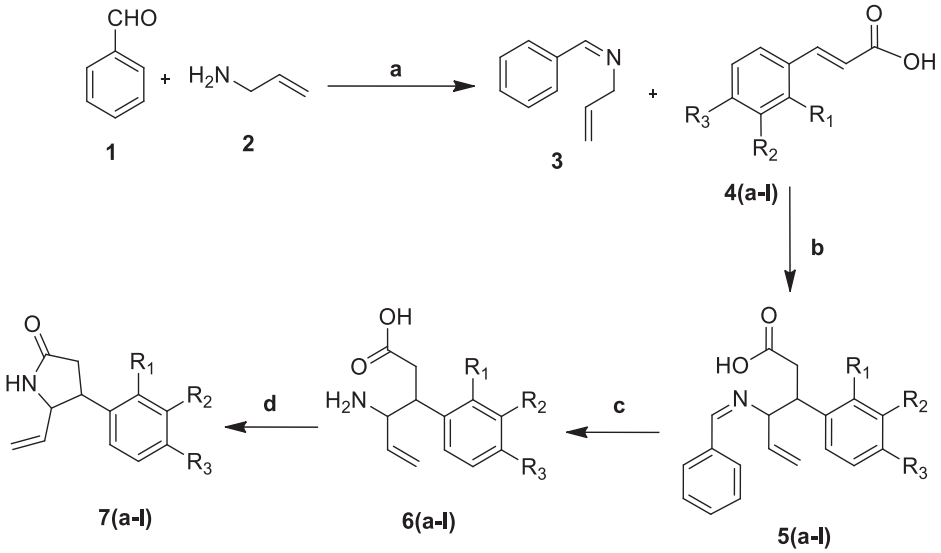

Scheme 1 Reagents and condition: (a) Na_2SO_4, DCM, Rt, 4 h (b) 50% NaOH, CH_3CN, TEBA, 0 °C, 1 h (c) aq. HCl, rt, 2 h (d) EDC, HOBt, 50 °C, 24 h

Table 1 List of substituted 4-phenyl-5-vinylpyrrolidin-2-one derivatives as novel GABA-AT inhibitors

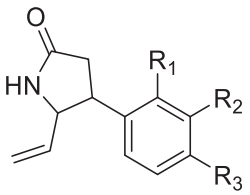

Compound	R_1	R_2	R_3
7a	H	H	NO_2
7b	H	NO_2	H
7c	NO_2	H	H
7d	H	H	H
7e	CF_3	H	H
7f	H	H	CF_3
7g	H	CF_3	H
7h	H	OH	H
7i	H	OH	OH
7j	OH	H	H
7k	H	H	OCH_3
7l	H	OCH_3	OCH_3

proton peak, and the appearance of characteristics singlet peak of one proton of benzylidenimine (–N=CH–) observed around 8.52 ppm. ^{1}H NMR spectra of all intermediates **5(a–l)** formed by the reaction of imine derivative (**3**) with cinnamic acid derivatives were confirmed by the presence of carboxylic acid proton (-COOH) as singlet around 12 ppm, methine proton peak of one proton at 4.5 instead of methylene (CH_2) protons doublet peak (present in 1 spectrum of derivative **3**). The compounds **6(a–l)** have shown the presence of two amines (NH_2) protons around 9 ppm, carboxylic acid proton (–COOH) as a singlet at around 12 ppm, and absence of 5 aromatic protons (present in **5(a-l)**). Finally, compounds **7(a–l)** exhibited the proton of methylene (=CH_2) and methine (=CH–) around ~6.40 ppm and ~5.30 ppm. The –NH group showed the integration of one proton in the range 4.83–7.71 ppm. The derivative (**7k** and **7l)** also appeared as a singlet peak of three protons of methoxy (-OCH_3) and six protons of dimethoxy at 4.22 ppm and 3.79, respectively. Compounds (**7h, 7i**, and, **7j)** exhibited a broad singlet proton peak of the phenolic hydroxyl (–OH) group in the range 5.52–9.07 ppm.

^{13}C NMR Spectral Analysis

^{13}C NMR spectral characterization was based on the presence of distinctive carbon peaks in the synthesized compounds (**3, 5(a–l), 6(a–l)**). The characteristic signals of N-allyl-1-phenylmethanimine (**3**) nucleus appeared for imine carbon (–C=N–) in the range of 160.0–162.1 ppm. All the intermediates **5(a-l)** exhibited characteristic signals of (–C=N–) and (>C=O) in the field of 160.0–162.1 ppm, and 177.0–179.0 ppm, along with the two aliphatic carbon (reaction centers) signals at 35.3–36.1 ppm and 63.5–66.2 ppm respectively. The compounds **6(a–l)** have shown the presence of a characteristic carbon signal (>C=O) at 177.0–179.0 ppm and the absence of 5 aromatic carbon signals (present in **5(a–l)**). Similarly, the final compounds **7(a–l)** have shown a peak of carbonyl (>C=O) group of pyrrolidin-2-one nuclei in the range of 166.89–180.23 ppm. The methylene (=CH_2) and methine (=CH–) proton of vinylic groups were in the range of 105.75–126.33 ppm and 122.61–140.78 ppm. The derivative of (**7k** and **7l)** were exhibited a peak of methoxy in the range of 52.20–55.60 ppm. These spectra have confirmed the presence of carbonyl groups and vinylic groups in 5-oxoisoxazolidine-2-carboxamide derivatives **7(a–l)**.

Table 2 Inhibitory constant and Log p of the synthesized compounds

Compound	IC_{50} value (μM) ± SEM	Log P[a]
7a	66.3 ± 0.32	1.650
7b	63.0 ± 0.22	1.407
7c	59.1 ± 0.31	1.553
7d	67.6 ± 0.34	1.710
7e	59.2 ± 0.46	2.588
7f	46.29 ± 0.31	1.650
7g	77.41 ± 0.24	1.237
7h	88.4 ± 0.31	1.407
7i	73.4 ± 0.45	1.650
7j	87.7 ± 0.41	1.395
7k	83.0 ± 0.37	1.333
7l	94.6 ± 0.36	2.588
Vigabatrin	41.93 ± 0.31	1.861

[a]Shake Flask Method

All the synthesized compounds were also evaluated by elemental analyses and results were found within the ±0.35% range of the theoretical values. The partition coefficient (Log P) values (Table 2) of the synthesized compounds **7(a–l)** were determined by the shake flask method using n-octanol/water. The melting points (uncorrected) of the targeted compounds were also determined. The R_f values of all the compounds were calculated using DCM: Methanol (8:2) as a solvent. The percentage purity of the synthesized compounds **7(a-l)** was determined on the Infinity II 1260 (Agilent, USA) HPLC system using Eclipse plus C8 column and methanol/water (90:10 v/v) mobile phase at the flow rate of 1 ml/min. The percentage purity of the compounds **7(a–l)** was determined and was ≥94%.

In-vitro analysis

GABA-AT inhibition assay

GABase enzyme obtained from Pseudomonas fluorescens, containing enzymes, i.e. Succinic semialdehyde dehydrogenase (SSADH) and GABA-aminotransferase (GABA-AT), were used for the in-vitro studies to estimate the potency and effectiveness of various derivatives. Enzyme inhibitory activity i.e. conversion of $NADP^+$ to NADPH was determined using a change in absorbance (at 340 nm). The derivatives **7(a-l)** were used for the estimation of IC_{50}. The compounds that possess electron-donating groups (-OH, $-OCH_3$) show a higher IC_{50} value than that of electron-withdrawing groups ($–NO_2$, CF_3) as shown in (Table 2). This showed that a decrease in electron density over γ-carbon that made it more susceptible to nucleophilic attack by Lys329. The increase in the value of IC_{50} with the substitution of the electron-donating group **7(h–l)** exhibited hydrophobic interaction with the enzyme but the inhibition may not be irreversible and revealed that is acting as a good substrate of the enzyme. The compound **7f** showed the lowest IC_{50} value amongst all derivatives and was further subjected to the estimation of inhibition constant K_i, which was determined with the fixed inhibitor concentration and varied substrate concentration. Further compound **7f** was incubated with the enzyme at its IC_{50} value shown in (Table 2).

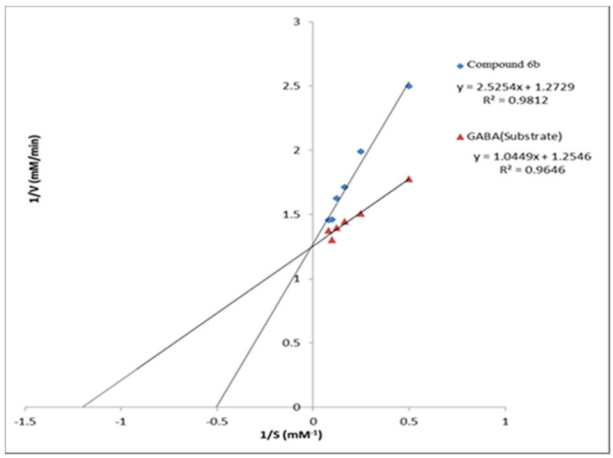

Fig. 2 Enzyme kinetic studies show competitive inhibition with the substrate (GABA)

The value of K_m observed for compound **7f** (1.983 μM) was comparable with GABA (0.833 μM), which showed that it could be a good substrate for GABA-AT, and competitive inhibition with GABA was also observed as shown graphically in (Error! Reference source not found.). The cheng-prusoff equation was used to determine the K_i value and was found to be 0.106 ± 0.004 μM which signifies the effectiveness of the compound at a low dose (Fig. 2).

Hydrolysis studies of compound 7f in a simulated biological fluid

The graph was plotted (Fig. 3) against the percentage of hydrolyzed drugs versus time interval. The linear plot showed that the percentage of hydrolyzed compound **7f** at gastric pH (1.2) is more in comparison to the compound at intestinal pH (6.8). This illustrated the stability of the compound at intestinal pH and hence will be available for its maximum absorption at intestinal pH. The mechanism of hydrolysis of the drug in the intestinal fluid is given in Fig. 4, which showed that the derivative **7f** undergoes hydrolysis in a basic medium and was converted into acyclic derivative which was analyzed through the λ_{max} values [14]. On enzymatic hydrolysis, the structure of the compound 6f mimics the standard Vigabatrin. The overall structure-activity relationship of the compounds has been presented in Fig. 5.

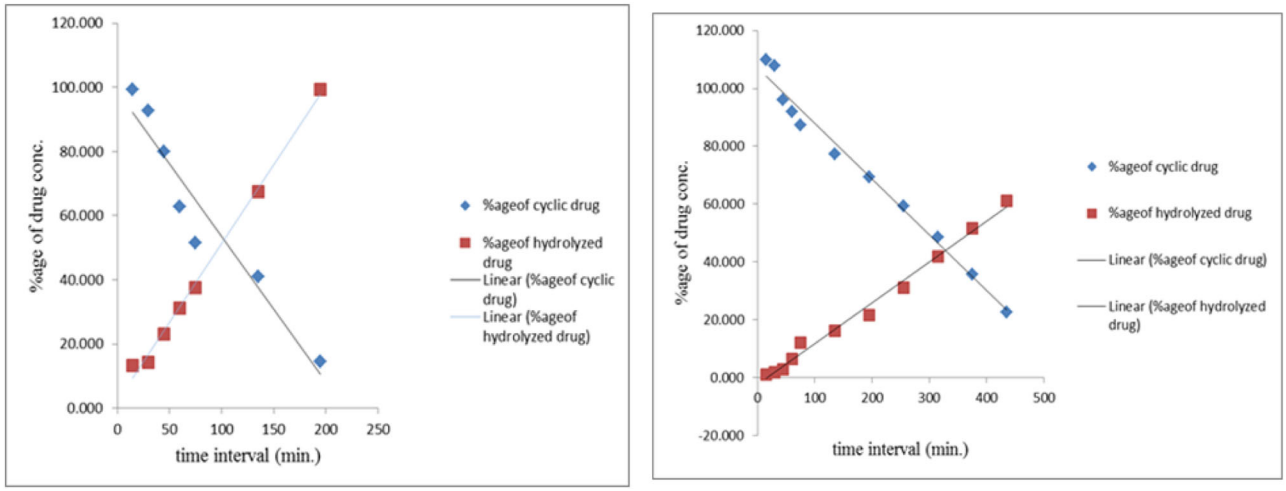

Fig. 3 Percentage hydrolysis of **7f** at simulated body fluid at pH 1.2 and pH 6.8

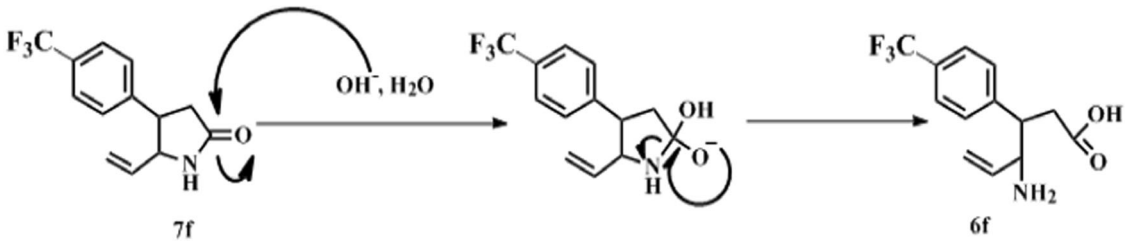

Fig. 4 Mechanism of intestinal hydrolysis of **7f**

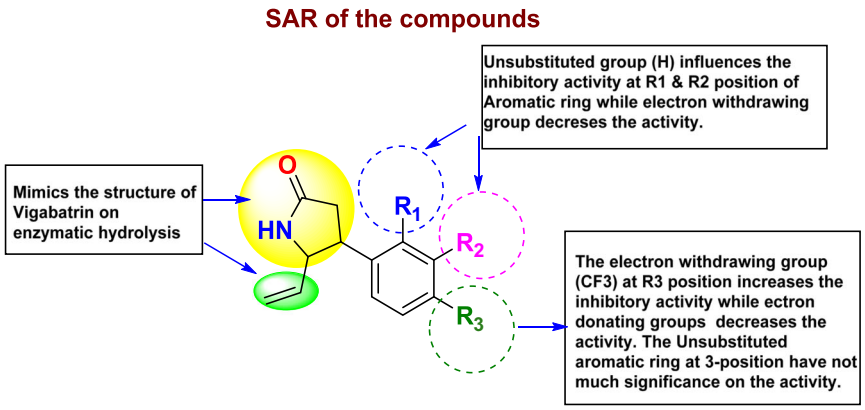

Fig. 5 Structure-activity relationship of the compounds

In-vivo evaluation

MES (Maximal Electroshock Induced Seizures) test and PTZ (Pentylenetetrazole) induced seizure test

The anticonvulsant activity was determined by MES (Maximal Electroshock Induced Seizures) test and PTZ (Pentylenetetrazole) induced seizures test. Vigabatrin (100 mg/Kg) and **7f** were (50, 100, 200 mg/Kg) were administered orally ad libitum. The one-way ANOVA test was performed followed by Kruskal–Wallis statistic test that showed $^{a}P < 0.05$ compared to Control (Vehicle), $^{b}P < 0.05$ compared to Diseased, $^{c}P < 0.05$ compared to Standard, and the insignificant difference in Vigabatrin (100 mg/Kg) and **7f** (200 mg/Kg) (Fig. 7).

There was a significant difference in the HLTE (Hind Limb Tonic Extensor) duration of the orally treated group in comparison to the control group (Fig. 6). The seizure duration and seizure latency signify the efficacy of the drug, and the results of effectiveness were insignificant with Vigabatrin. The similar response of compound **7f** shows a decrease in seizure duration, which

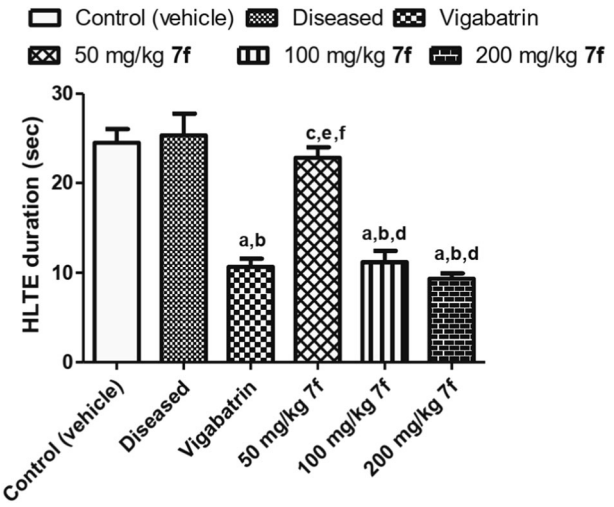

Fig. 6 Comparison of HLTE duration among Control, Standard, and 7f Groups. All Values are Mean ± SD. $^{a}P < 0.05$ compared to Control (Vehicle), $^{b}P < 0.05$ compared to Diseased, $^{c}P < 0.05$ compared to Standard. [ANOVA (one-way) followed by Kruskal–Wallis statistic test]

signifies that the molecule is active as an anti-convulsant agent (Fig. 7).

Biochemical estimation of GABA

Further, the increase in the level of GABA concentration was measured. The rats were stereotaxically treated with Vigabatrin and compound **7f** icv. After 18 hr of surgery, rats were subjected to an MES test. The treated rats show a relatively fast recovery time in MES in the test compound as compared to the control and sham group (placebo surgery group) as shown in (Fig. 8), which signifies the increase in the level of GABA in the cortical region which may minimize the intensity of seizures. The level of GABA increased in the standard Vigabatrin group and test compound **7f** group to that of the control and sham group. It was reported that there is an increase in the level of GABA and that was due to the binding of Vigabatrin with the GABA-AT (inhibition of GABA-AT); because of the prevention of its metabolism, it reflects that the compound **7f** also raises the level of GABA by inhibiting

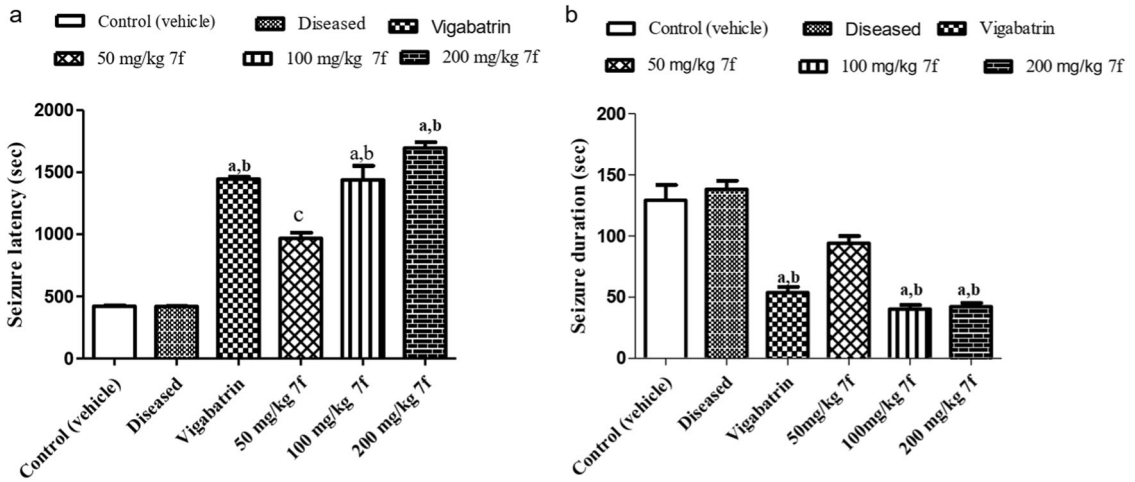

Fig. 7 Comparison of (**a**) Seizure Latency and (**b**) Seizure Duration among Control, Standard, and 7f Groups. All Values are Mean ± SD. $^{a}P < 0.05$ compared to Control (Vehicle), $^{b}P < 0.05$ compared to Diseased, $^{c}P < 0.05$ compared to Standard. [ANOVA (One-way) followed by Kruskal–Wallis statistic test]

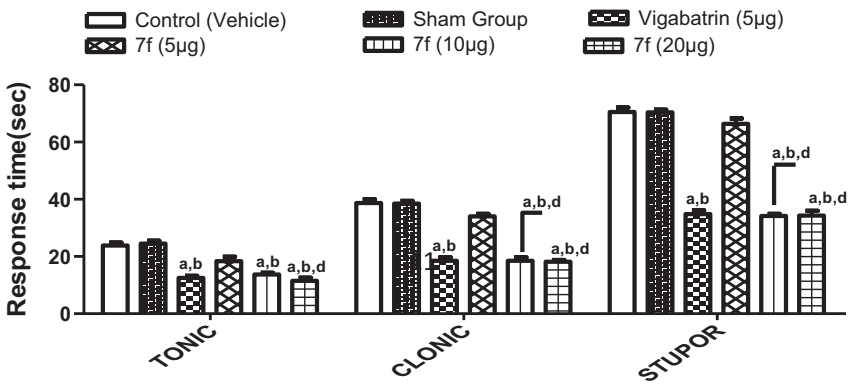

Fig. 8 Effect on response time among the six treatment group at 18 h in the MES model. All Values are Mean ± SD. $^{a}P < 0.05$ compared to Control (Vehicle), $^{b}P < 0.05$ compared to Sham group, $^{c}P < 0.05$ compared to Vigabatrin, $^{d}P < 0.05$ compared to 7f (5 µg), $^{e}P < 0.05$ compared to 7f (10 µg) $^{f}P < 0.05$ compared to 7f (20 µg) [ANOVA (Two-way) followed by Bonferroni Post-hoc test]

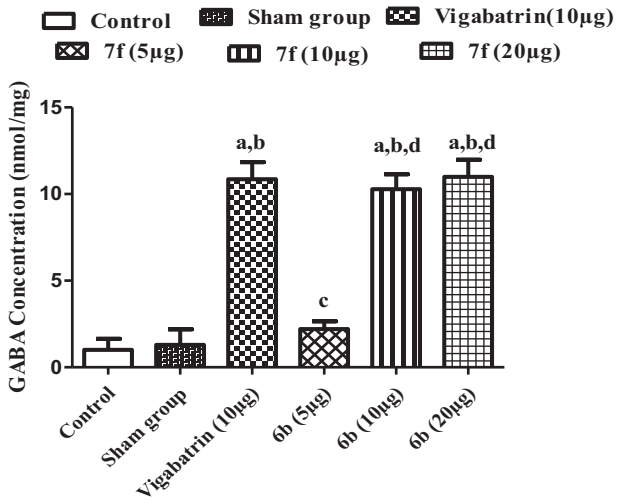

Fig. 9 GABA concentration (nmol/mg) among the six treatment group after 18 h of administration. All values are Mean ± SD. $^{a}P < 0.05$ compared to control, $^{b}P < 0.05$ compared to Sham group, $^{c}P < 0.05$ compared to Vigabatrin (10 µg), $^{d}P < 0.05$ compared to 7f (5 µg), $^{e}P < 0.05$ compared to 7f (10 µg) $^{f}P < 0.05$ compared to 7f (20 µg). [ANOVA (Two-way) followed by Bonferroni Post-hoc test]

GABA-AT. The cortical region was excised and spectrofluorometric estimation of GABA concentration was made. The ANOVA (Two-way) test followed by Bonferroni Post-hoc test was applied and it was found that $^{a}P < 0.05$ as compared to control, $^{b}P < 0.05$ as compared to Sham group, $^{c}P < 0.05$ as compared to Vigabatrin (10 µg), $^{d}P < 0.05$ as compared to **7f** (5 µg), $^{e}P < 0.05$ as compared to **7f** (10 µg) $^{f}P < 0.05$ as compared to **7f** (20 µg). The increase in the level of GABA was significant with the Vigabatrin at dose 5 µg but was comparable /insignificant at 10 µg and 20 µg which shows that the compound synthesized has similar potency as compared to Vigabatrin. The graphical representation of the change in the level of GABA among the six treatment groups was presented in (Fig. 9).

Histopathological examination of PTZ treated rat brains

The hippocampal part of the rat brain treated with PTZ and test compound was embedded into 10% formalin for microtoming of tissues and preparation of thin slices of hippocampal neurons. The thin slices of the hippocampus were treated with dye Cresyl-Fast (violet stain) for Nissl staining (highlight neuron structural features) and observed under photomicroscope for any tissue damage as well as morphological changes [15]. The hippocampal tissue of control rats revealed that the tissue morphology and vasculature appeared normal. The PTZ-treated group of rats has shown pathological alteration (necrosis) in tissue. Whereas in the treated group, necrosis tissue areas have been significantly reduced. These histological observations which were marked by reduced induction of seizure also confirm the biochemical findings (Fig. 10).

In-silico studies

Molecular docking studies

Re-docking the co-crystallized ligand into their respective grid confirmed the docking parameters and produced grid at first. To confirm the suitability of docking techniques and generated grid, the superposition tool was employed, which exhibited RMSD values within two between co-crystallized and re-docked ligand as shown in fig.37 of supplementary data. The highest G-Score value was obtained for compound **7f** among all other derivatives. The computational results indicated that **7f** and Vigabatrin were correctly positioned in the enzyme cleft and showed interaction with the internal amino acid residues Phe189, His190, Gly191, Asp298, Glu299, Val300, Gln301, Thr302, Lys329, and PLP600. The benzene ring of **7f** displayed π-π and hydrogen interaction with the Phe189. The carbonyl group is involved in the formation of the hydrogen bond with Gly136, NH group showed charged interaction with Lys329. In-silico studies were found to agree with the in-vitro studies and revealed **7f** as the most active compound (Fig. 10). From the G-score value, it can be evaluated that the substitution at the para-position of the phenyl ring with an electron-withdrawing group increases the susceptibility towards active site binding residues [16].

Whereas the same group at –o and –m positions show low G-score but the values are still comparable. The electron-donating group shows that increasing the electron density conversely increases the hydrophobic interaction with the enzyme. An increase in the number of electrons donating substituents decreases the G-score value [17].

Molecular dynamics simulations

To evaluate the stability and possible binding mode of the ligands in the docked complex, we performed an MD simulation of compound **7f** for 50 ns. The structural stability of the docked complex was evaluated using root mean square deviation (RMSD). As formed (Fig. 11 & Fig. 12), it could be inferred that initially, up to 5 ns time scale, the fluctuations were observed between the protein backbone and docked ligand complex. After the 5 ns, the trajectory of the protein backbone was found to be stable in the active site of the protein with a mean value of 2.0 Å. The root means square fluctuations were analyzed and observed the lesser fluctuations of active site residues of the enzyme with compound **7f** (Fig. 13).

Protein-ligand interactions during the simulation run time were also evaluated. The exchanges are classified by Hydrophobic, Hydrogen Bonds, Ionic, and Water Bridges

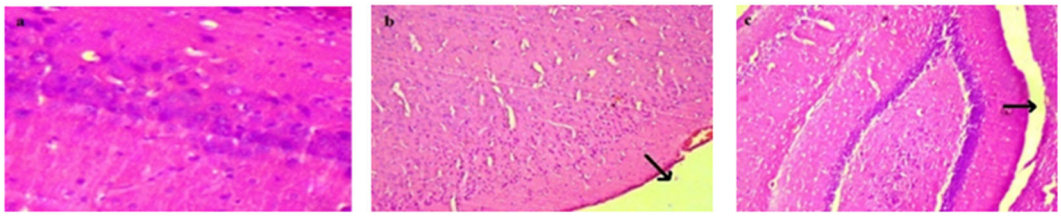

Fig. 10 Histopathological photographs of Hippocampal Tissue of rat brain of the control group, PTZ treated group and **7**f treated a group

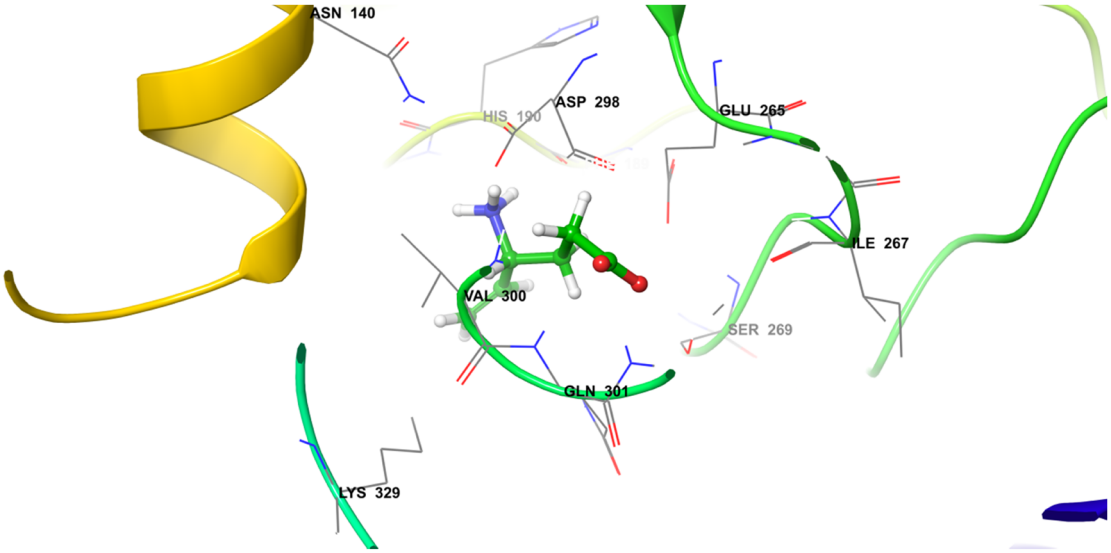

Vigabatrin

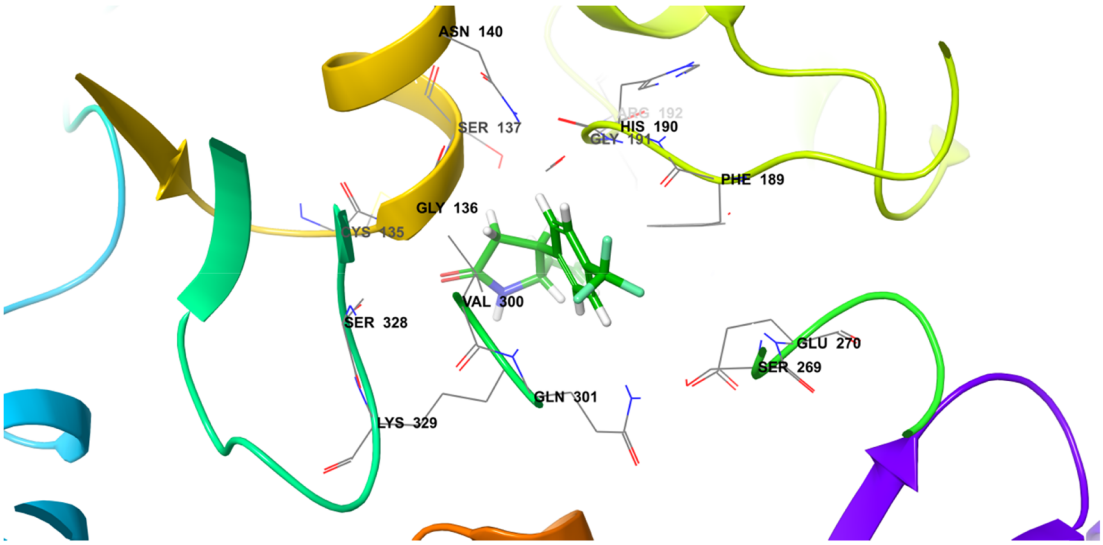

7f

Fig. 11 Binding modes of Vigabatrin and 7f in the GABA-AT binding pocket (PDB: 1OHW) with PLP as a cofactor

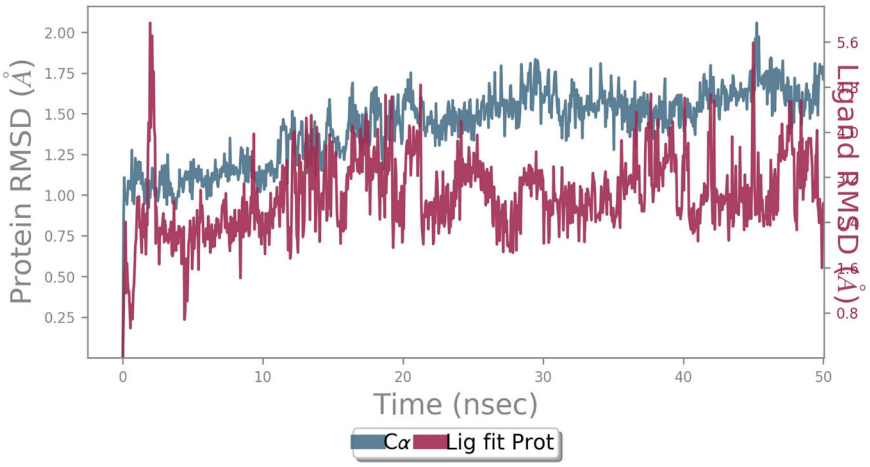

Fig. 12 RMSD graph of the compound (7f) and GABA-AT binding pocket (PDB: 1OHW) enzyme complex for the period of 50 ns simulation

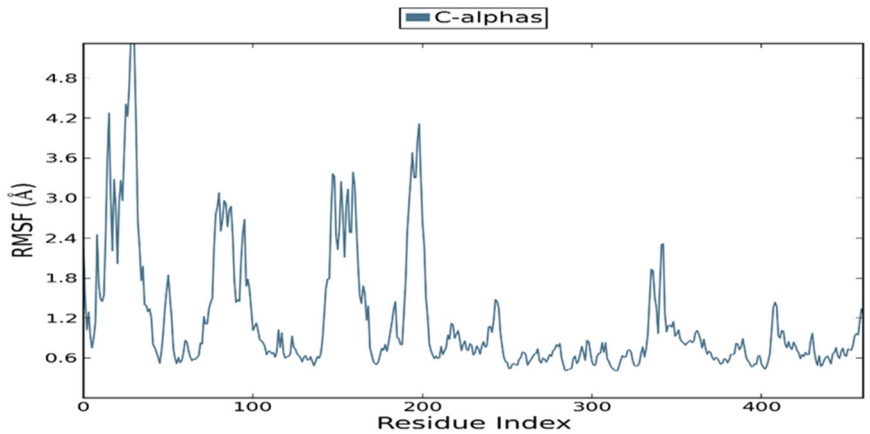

Fig. 13 RMSF graph of the compound 7f and GABA-AT binding pocket (PDB: 1OHW) enzyme complex for the period of 50 ns simulation

and shown as a histogram in (Fig. 14) the results showed that amino acid residues His206, Arg192, Glu270, and Lys 329 contribute to the interaction pattern. Arg192 showed hydrogen bonding, Glu270 showed hydrogen bonding, ionic and water bridge interaction during the MD simulation time. The interactions observed in the docking analysis were also found to retain throughout the simulation time.

MMGB-SA & ADME prediction

The MM-GBSA analysis of the compound **7f** was carried out to predict the binding free energy of docked ligand into the respective protein. The results of MM-GBSA analysis (Fig. 38, Supporting Information) showed compound **7f** and vigabatrin with the minimum binding free energy of -16 and -18 kcal/mol for GABA-AT, respectively.

The QikProp module of Schrodinger was used to evaluate compound **7f** for drug-likeliness properties, and the results were determined (Fig. 38, Supporting Information). The outcome of Lipinski's rule of five (mol_MW < 500, QPlog Po/w < 5, donorHB 0–6.0, accptHB 2.0–20), along with the other predicted parameters (SASA 300-1000, Mol logP 3.30, pKa of most Basic/Acidic group 3.01 / 9.02, BBB Score 4.93 (6-High,0-Low)) reflected that the compound **7f** elicited the"drug-like" properties.

Conclusion

Compounds 4-phenyl-5-vinylpyrrolidin-2-one derivatives act as a good substrate for GABA-AT. The compound **7f** has comparable potency with Vigabatrin. The electron-donating substituents over the aromatic ring of the compound contributed to increasing hydrophobic interactions with the enzyme active site, but the susceptibility of nucleophilic attack decreases whereas the electron-withdrawing groups decrease the availability of electrons at γ-C-H and hence make it more prone to Lys329 interaction which results in irreversible inhibition of the enzyme. The compound **7f** was effective at a low dose but had comparable activity as Vigabatrin. The stability in gastric pH and lipophilicity of the synthesized compound can minimize the bioavailability problem of Vigabatrin with increased intestinal and blood-brain barrier absorption which can be further estimated in the future.

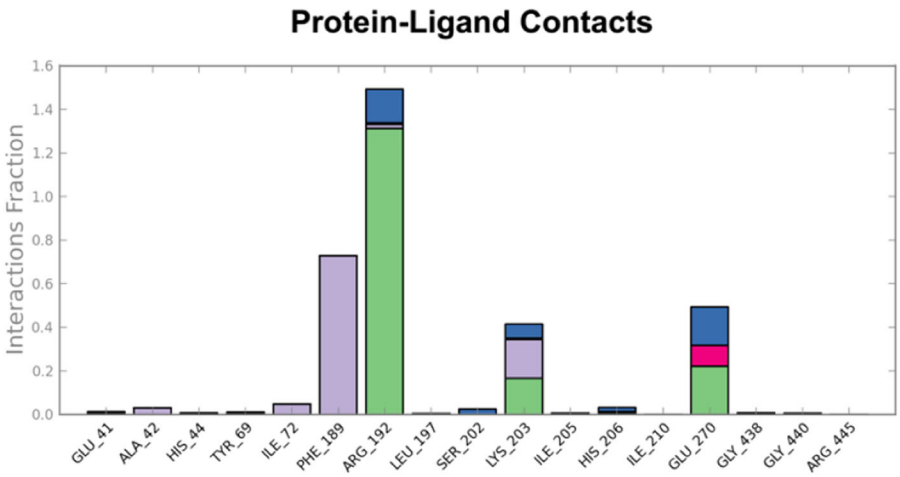

Fig. 14 Protein-ligand contacts through 50 ns simulation of compound 7f and GABA-AT binding pocket

Experimental section

Chemistry

Instrumentation and chemicals

Chemicals and reagents: All the chemicals and reagents were purchased from Sigma-Aldrich chemicals and Avra Synthesis Pvt. Ltd. Solvents were purchased from Merck Millipore. Melting points (uncorrected) were determined in open capillary tubes using a heating block type melting point apparatus (Lab India). Completion of the reactions was monitored by, silica gel 60 F254 aluminum sheets; precoated thin layer chromatography (TLC) plates (Merck, Germany), and spots were visualized in ultraviolet light and/or iodine vapors. FT-IR spectra were recorded on a Shimadzu 8400S FT-IR spectrophotometer. ^{1}H NMR (500 MHz) was recorded on a Brucker FT-NMR in DMSO-d_6 using TMS as an internal standard. C, H, and N analyses were performed on an Exeter CE-440 elemental analyzer. Mass spectra were recorded on LC-Q-TOF mass spectrophotometer with an ESI source (Agilent Infinity II 1290 LC). Partition coefficient was determined on rotary flask shaker by shake flask method [18]. Vigabatrin was used as a standard and it was purchased from Sigma-Aldrich.

Synthesis

The general procedure of synthesis of intermediate 3 To a solution of benzaldehyde (2.5 mmol) in dry dichloromethane (15 mL) was added anhydrous sodium sulfate (5 mmol, 2 equiv.) and allylamine (2.5 mmol,1 equiv.) the resulting suspension was stirred for one hour at room temperature. After completion of the reaction, sodium sulfate was removed by filtration, and the solvent evaporated under a vacuum. The concentrated liquid was used as such in the next step without any further purification [19].

General procedure for the synthesis of 5(a-l) The liquid obtained in the first step was cooled to 0 °C and a solution of a cinnamic acid derivative **4(a–l)** (5 mmol) and TEBA benzyltriethylammonium chloride (0.25 mmol) in 2.5 mL acetonitrile was added to it. The resultant solution was stirred at 0 °C and then cooled aqueous sodium hydroxide (50%, 1.5 mL) was added to it. The reaction mixture was stirred until crystallization began (7–40 min) and then it was kept for 1 h at 0 °C. 100 mL water was added, and the solid was collected and washed with water until the compound became neutral and then recrystallized from ethanol to give white crystals [20].

General procedure for the synthesis of 6(a-l) Hydrochloric acid (20 ml, 10%) was added to **5(a-l)** and stirred at room temperature for 2 h. The precipitate was collected, washed with brine solution, and recrystallized from ethanol to yield white crystals [20].

4-amino-3-(4-nitrophenyl)hex-5-enoic acid (6a):

Brown solid; yield 38%; IR spectra (KBr disc method, cm^{-1}): 1731.00 (>C=O_{str}), 3478.51 (-NH_{2str}); ^{1}H NMR (500 MHz, DMSO-d_6, δ_H): 2.10 (s, 2H, –NH_2), 2.46 (m, 2H, –CH_2), 3.66 (s, 1H, -CH), 3.96 (s, 1H, –CH), 6.49–6.59 (m, 2H, =CH_2), 6.78 (s, 1H, =CH), 7.78 - 8.23 (m, 4H, H-Ar), 12.59 (brs, 1H, –OH); Anal. $C_{12}H_{14}N_2O_4$: C, 57.59; H, 5.64; N, 11.19; Found: C, 57.61; H, 5.63; N, 11.25.

4-amino-3-(3-nitrophenyl)hex-5-enoic acid (6b):

Pale white solid; yield 42%; IR spectra (KBr disc method, cm^{-1}): 1712.49 (>C=O_{str}), 3448.84 (-NH_{2str}); ^{1}H NMR (500 MHz, DMSO-d_6, δ_H): 2.11 (s, 2H, -NH_2), 2.54 (m, 2H, –CH_2), 3.65 (s, 1H, –CH), 3.90 (s, 1H, –CH), 6.49–6.61 (m, 2H, =CH_2), 6.78 (s, 1H, =CH),

7.67–8.02(m, 4H, H-Ar), 12.60 (brs, 1H, –OH); Anal. $C_{12}H_{14}N_2O_4$: C, 57.59; H, 5.64; N, 11.19; Found: C, 57.58; H, 5.60; N, 11.10.

4-amino-3-(2-nitrophenyl)hex-5-enoic acid (6c):

White solid; yield 57%; IR spectra (KBr disc method, cm^{-1}): 1712.49 (>C=O_{str}), 3448.84 (-NH_{2str}); ^1H NMR (500 MHz, DMSO-d_6, δ_H): 2.13 (s, 2H, –NH_2), 2.51 (m, 2H, –CH_2), 3.65 (s, 1H, –CH), 3.96 (s, 1H, –CH), 6.52–6.56 (m, 2H, =CH_2), 6.72 (s, 1H, =CH), 7.78–7.88 (m, 4H, H-Ar), 12.62 (brs, 1H, –OH); Anal. $C_{12}H_{14}N_2O_4$: C, 57.59; H, 5.64; N, 11.19; Found: C, 57.60; H, 5.65; N, 11.18.

4-amino-3-phenylhex-5-enoic acid (6d):

Brownish solid; yield 64%; IR spectra (KBr disc method, cm^{-1}); 1749.49 (>C=O_{str}), 3263.66–3360.11 (NH_{2str}); ^1H NMR (500 MHz, DMSO-d_6, δ_H): 2.09 (s, 2H, –NH_2), 2.51 (m, 2H, –CH_2), 3.35 (s, 1H, –CH), 4.16 (s, 1H, –CH), 6.52–6.85 (m, 2H, =CH_2), 6.85 (s, 1H, =CH), 7.42–7.58 (m, 5H, H-Ar), 12.41 (brs, 1H, –OH); Anal. $C_{12}H_{15}NO_2$: C, 70.22; H, 7.37; N, 6.82; Found: C, 70.15; H, 7.34; N, 6.80.

4-amino-3-(2-trifluoromethyl)phenyl)hex-5-enoic acid (6e):

Yellow solid; yield 54%; IR spectra (KBr disc method, cm^{-1}): 1750.04 (>C=O_{str}), 3454.44 (-NH_{2str}); ^1H NMR (500 MHz, $CDCl_3$, δ_H): 2.56 (s, 2H, -NH_2), 3.12 (d, $J = 7$ Hz, 2H, -CH_2), 3.41 (d, $J = 8$ Hz, 2H, -CH benzyl,-CH vinyl), 6.59 (m, 2H, =CH_2), 6.79 (d, 1H, =CH), 7.52–8.16 (m, 4H, H-Ar), 12.41 (brs, 1H, -OH); Anal. $C_{13}H_{14}F_3NO_2$: C, 57.14; H, 5.16; N, 5.13; Found: C, 57.30; H, 5.14; N, 5.14.

4-amino-3-(4-trifluoromethyl)phenyl)hex-5-enoic acid (6f):

White solid; yield 39%; IR spectra (KBr disc method, cm^{-1}): 1745.84 (>C=O_{str}); 3265.45–3369.00 (–NH_{2str}); ^1H NMR (500 MHz, $CDCl_3$, δ_H): 2.51 (s, 2H, –NH_2), 3.45 (d, $J = 7.5$ Hz, 2H, -CH_2), 3.89 (d, $J = 8$ Hz, 2H, –CH benzyl, –CH vinyl), 6.21 (m, 2H, =CH_2), 6.42 (d, $J = 6$ Hz, 1H, =CH), 7.54-8.10 (m, 4H, H-Ar), 12.54 (brs, 1H, –OH); Anal. $C_{13}H_{14}F_3NO_2$: C, 57.14; H, 5.16; N, 5.13; Found: C, 57.21; H, 5.16; N, 5.11.

4-amino-3-(3-trifluoromethyl)phenyl)hex-5-enoic acid (6g):

Yellow solid; yield 42%; IR spectra (KBr disc method, cm^{-1}): 1735.39 (>C=O_{str}); 3210.26–3356.89 (-NH_{2str}); ^1H NMR (500 MHz, $CDCl_3$, δ_H): 2.24 (s, 2H, –NH_2), 3.45 (d, $J = 7.5$ Hz, 2H, –CH_2), 3.89 (d, $J = 8$ Hz, 2H, -CH benzyl, –CH vinyl), 6.57 (m, 2H, =CH_2), 6.71 (d, $J = 7$ Hz, 1H, =CH), 7.52–8.07 (m, 4H, H-Ar), 12.52 (brs, 1H, –OH); Anal. $C_{13}H_{14}F_3NO_2$: C, 57.14; H, 5.16; N, 5.13; Found: C, 57.05; H, 5.15; N, 5.14.

4-amino-3-(3-hydroxyphenyl)hex-5-enoic acid (6h):

Brown solid; yield 51%; IR spectra (KBr disc method, cm^{-1}): 1743.71 (>C=O_{str}), 3072.71–3288.74 (–NH_{2str}), 3381.33 (–OH_{str}); ^1H NMR (500 MHz, DMSO-d_6, δ_H): 2.23 (s, 2H, –NH_2), 2.51 (m, 2H, –CH_2), 3.34 (s, 1H, –CH), 3.59 (s, 1H, –CH), 6.81 (s, 1H, –OH), 6.82 (d, $J = 8.3$ Hz, 2H, =CH_2), 6.83 (s, 1H, =CH), 7.00–7.08 (m, 4H, H-Ar), 12.51 (brs, 1H, –OH); Anal. $C_{12}H_{15}NO_3$: C, 65.14; H, 6.83; N, 6.33; Found: C, 65.35; H, 6.81; N, 6.34.

4-amino-3-(3,4-dihydroxyphenyl)hex-5-enoic acid (6i):

Light brown solid; yield 56%; IR spectra (KBr disc method, cm^{-1}): 1742 (>C=O_{str}); 3245.32 - 3354.00 (–NH_{2str}), 3412.28 (–OH_{str});^1H NMR (500 MHz, $CDCl_3$, δ_H): 2.45 (s, 2H, –NH_2), 3.41 (d, $J = 4.2$ Hz, 2H, –CH_2), 3.74 (d, $J = 7.7$ Hz, 2H, –CH benzyl, –CH vinyl), 6.23 (m, 2H, =CH_2), 6.71 (brs, 2H, –OH), 6.79 (d, $J = 3.4$ Hz, 1H, =CH), 7.15–7.68 (m, 3H, H-Ar), 12.64 (brs, 1H, –OH); Anal. $C_{12}H_{15}NO_4$: C, 60.75; H, 6.37; N, 5.90; Found: C, 60.70; H, 6.36; N, 5.91.

4-amino-3-(2-hydroxyphenyl)hex-5-enoic acid (6j):

Brown solid; yield 69%; IR spectra (KBr disc method, cm^{-1}): 1741 (>C=O_{str}), 3156.32–3242.12 (–NH_{2str}), 3374.13 (–OH_{str}); ^1H NMR (500 MHz, DMSO-d_6, δ_H): 2.45 (s, 2H, –NH_2), 2.98 (m, 2H, –CH_2), 3.79 (m, 1H, –CH), 3.87 (d, $J = 8.2$ Hz, 1H, –CH), 6.85 (s, 1H, –OH), 6.78 (d, $J = 9$ Hz 2H, =CH_2), 6.84 (s, 1H, = CH), 7.10–7.28 (m, 4H, H-Ar), 12.54 (brs, 1H, –OH); Anal. $C_{12}H_{15}NO_3$: C, 65.14; H, 6.83; N, 6.33; Found: C, 65.215; H, 6.85; N, 6.31.

4-amino-3-(4-methoxyphenyl)hex-5-enoic acid (6k):

Red solid; yield 41%; IR spectra (KBr disc method, cm^{-1}): 1749.49 (>C=O_{str}), 3200.01–3456.55 (–NH_{2str}); ^1H NMR (500 MHz, DMSO-d_6, δ_H): 2.13 (s, 2H, –NH_2), 2.52 (m, 2H, –CH_2), 3.27 (m, 1H, –CH), 3.54 (d, $J = 7.4$ Hz, 1H, –CH), 3.80 (s, 3H, –OCH_3), 6.35 (d, $J = 8$ Hz, 2H, =CH_2), 6.97 (d, $J = 10$ Hz, 1H, =CH), 7.53–7.65 (m, 4H, H-Ar), 12.63 (brs, 1H, –OH); Anal. $C_{13}H_{17}NO_3$: C, 66.36; H, 7.28; N, 5.95; Found: C, 66.21; H, 7.26; N, 5.98.

4-amino-3-(3,4-dimethoxyphenyl)hex-5-enoic acid (6l):

Dark brown solid; yield 45%; IR spectra (KBr disc method, cm^{-1}): 1747.21 (>C=O_{str}), 3210.01–3438.41 (–NH_{2str}); ^1H NMR (500 MHz, DMSO-d_6, δ_H): 2.59 (s, 2H, –NH_2), 2.74 (m, 2H, –CH_2), 3.28 (m, 1H, –CH), 3.59 (d, $J = 6.4$ Hz, 1H, –CH), 3.89 (s, 6H, –OCH_3), 6.31 (d, $J = 5.3$ Hz, 2H, = CH_2), 6.99 (d, $J = 7.2$ Hz, 1H, =CH), 7.20–7.53 (m, 3H, H-Ar), 12.51 (brs, 1H, –OH); Anal. $C_{14}H_{19}NO_4$: C, 63.38; H, 7.22; N, 5.28; Found: C, 63.30; H, 7.20; N, 5.28.

General procedure for the synthesis of 7(a-l) The recrystallized product **6(a–l)** was dissolved in THF with vigorous stirring. EDC and HOBt were added to the THF solution and mixed uniformly. The reaction mixture was refluxed at 50 °C under an N_2 atmosphere for 24 h. On reaction completion, the reaction mixture was cooled and filtered out. The solvent was evaporated and the residue was dissolved in DCM. The organic solvent was washed with 5% HCl, sodium bicarbonate, and brine solution and then the solvent

was evaporated. The product was recrystallized from cold ethyl acetate.

4-(4-nitrophenyl)-5-vinylpyrrolidin-2-one (7a):

Pale white solid; yield 49%; m.p. 125–126 °C; UV(λ_{max}) 339.26 nm; IR spectra (KBr disc method, cm^{-1}): 1685.84, 1539.25, 850.64, 987.59, 1109.11, 671.25, 1228.70, 1352.14, 3431.48; ^{1}H NMR (DMSO-d_6, 500 MHz, δ_H): 4.33 (s, 2H, –CH_2), 5.09 (s, 2H, -CH benzyl,-CH vinyl), 5.25(dd, $J = 6$ Hz, 2H, –CH_2 of vinyl), 6.75 (s, 1H, -NH), 7.69 (q, $J = 50$ Hz, 1H, –CH of vinyl), 7.966 (d, 2H, aromatic region), 8.241 (d, 2H, aromatic region);^{13}C NMR (DMSO-d_6, 125 MHz, δ_C): 167.025, 147.924, 141.221, 140.778, 132.817, 129.286, 129.242, 128.547, 123.927, 123.748, 57.738, 44.981, 30.690. Anal. $C_{12}H_{12}N_2O_3$: C,62.06; H,5.21; N,12.06; O,20.67; Found: C,62.04; H,5.22; N,12.08; O,20.66. LC/MS (ESI, *m/z)*: 232.12 $[M + H]^+$.

4-(3-nitrophenyl)-5-vinylpyrrolidin-2-one (7b):

Pale white solid; yield 80%; m.p. 155–158 °C; UV(λ_{max}) 318.15 nm; IR spectra (KBr disc method, cm^{-1}): 1637.62, 1535.39, 827.49, 925.86, 1228.70, 744.55, 1618.33, 1359.86, 3452.70; ^{1}H NMR ($CDCl_3$, 500 MHz, δ_H): 3.273 (s, 2H, –CH_2), 3.583 (s, 2H, –CH linked to benzyl and CH linked to vinyl), 4.188 (dd, $J = 8.5$ Hz, 18 Hz, 2H, –CH_2 of vinyl), 4.778 (q, 1H, -CH of vinyl), 6.553 (s, 1H, -NH), 7.491-7.684 (m, 4H, aromatic region); ^{13}C NMR (DMSO-d_6, 125 MHz, δ_C): 167.067, 148.303, 141.394, 136.128, 133.973, 130.306, 124.320, 122.738, 122.302, 57.738, 44.981, 30.612. Anal. $C_{12}H_{12}N_2O_3$: C,62.06; H,5.21; N,12.06; O,20.67; Found: C,62.04; H,5.23; N,12.09; O,20.64. LC/MS (ESI, *m/z)*: 232.03 $[M + H]^+$.

4-(2-nitrophenyl)-5-vinylpyrrolidin-2-one (7c):

Pale white solid; yield 50%; m.p. 145–147 °C; UV(λ_{max}) 289.26 nm; IR spectra (KBr disc method, cm^{-1}): 3259.81, 1707.06, 1545.03, 1514.17, 1384.94, 1024.24, 987.59, 833.28, 698.25; ^{1}H NMR ($CDCl_3$, 500 MHz, δ_H): 3.4775(d, $J = 8.5$ Hz, 2H, –CH_2), 3.836 (s, 2H, –CH linked to benzyl and -CH linked to vinyl), 4.049 (dd, $J = 7.5$ Hz,18 Hz, 2H, -CH_2 of vinyl), 4.833 (q, $J = 20$ Hz, 1H, -CH of vinyl), 6.369 (s,1H, -NH), 7.641-8.140 (m, 4H, aromatic region); ^{13}C NMR ($CDCl_3$, 125 MHz, δ_C): 179.977, 162.067, 146.336, 143.645, 130.121, 129.796, 117.314, 114.601, 55.594, 33.031, 31.132. Anal. $C_{12}H_{12}N_2O_3$: C,62.06; H,5.21; N,12.06; O,20.67; Found: C,62.05; H,5.19; N,12.10; O,20.66. LC/MS (ESI, *m/z)*: 232.09 $[M + H]^+$

4-phenyl-5-vinylpyrrolidin-2-one (7d):

Pale white solid; yield 48%; m.p. 160-162 °C; UV(λ_{max}) 278.50 nm; IR spectra (KBr disc method cm^{-1}): 3321.53, 2928.04, 1624.12, 1541.18, 1458.23, 1087.89, 763.84, 669.32; ^{1}H NMR ($CDCl_3$, 500 MHz, δ_H): 2.577 (d, $J = 8.5$ Hz, 2H, –CH_2), 2.836 (s, 2H, –CH linked to benzyl and -CH linked to vinyl), 3.427 (dd, $J = 6.5$ Hz 10.5 Hz, 2H, –CH_2 of vinyl), 4.833 (q, $J = 20$ Hz, 1H, –CH of vinyl), 6.369 (s, 1H, -NH), 7.261-7.818 (m, 5H, aromatic region); ^{13}C NMR ($CDCl_3$, 125 MHz, δ_C): 178.035, 157.375, 129.138, 128.289, 126.728, 125.253, 119.842, 49.557, 33.999, 31.120. Anal. $C_{12}H_{13}NO$: C,76.98; H,7.00; N,7.48; O,8.54; Found: C,76.94; H,6.98; N,7.51; O,8.57. LC/MS (ESI, *m/z)*: 187.14 $[M + H]^+$.

4-(2-(trifluoromethyl)phenyl)-5-vinylpyrrolidin-2-one (7e):

Pale white solid; yield 56%; m.p. 222–224 °C; UV(λ_{max}) 298.35 nm; IR spectra (KBr disc method, cm^{-1}): 3358.18, 1631.83, 1313.57, 1163.11, 941.29, 765.77, 545.87; ^{1}H NMR ($CDCl_3$, 500 MHz, δ_H): 3.477 (d, $J = 8.5$ Hz, 2H, –CH_2), 3.836 (s, 2H, –CH linked to benzyl and -CH linked to vinyl), 4.194 (dd, $J = 5.5$ Hz, 8 Hz, 2H, –CH_2 of vinyl), 4.833 (q, 1H, -CH of vinyl), 6.369 (s, 1H, –NH), 7.243–7.695(m, 4H, aromatic region); ^{13}C NMR ($CDCl_3$, 125 MHz, δ_C): 180.229 (1 C, –C=O group), 141.276, 132.292, 129.818, 128.210, 126.329, 61.267, 50.267, 31.082. Anal. $C_{13}H_{12}F_3NO$: C,61.17; H,4.74; F,22.33; N,5.49; O,6.27; Found: C,61.20; H,4.71; F,22.35; N,5.46; O,6.28. LC/MS (ESI, *m/z)*: 255.0 $[M + H]^+$.

4-(4-(trifluoromethyl)phenyl)-5-vinylpyrrolidin-2-one (7f):

Pale white solid; yield 60%; m.p. 215–217 °C; UV(λ_{max}) 258.15 nm; IR spectra (KBr disc method, cm^{-1}): 1637.62, 949.01, 1168.90, 1338.64, 810.13, 596.02, 3452.70; ^{1}H NMR ($CDCl_3$, 500 MHz, δ_H): 2.946 (s, 2H, –CH_2), 3.207 (d, $J = 38.5$ Hz, 2H, –CH linked to benzyl and –CH linked to vinyl), 4.1965 (dd, $J = 5.5$ Hz, 8 Hz, 2H, –CH_2 of vinyl), 4.833 (q, $J = 20$ Hz, 1H, –CH of vinyl), 6.369 (s, 1H, –NH), 7.499–7.693 (m, 4H, aromatic region); ^{13}C NMR ($CDCl_3$, 125 MHz, δ_C): 171.294, 145.184, 135.192, 132.011, 131.752, 131.447, 129.755, 127.241, 125.130, 122.893, 119.725, 52.203, 49.277, 29.914. Anal. $C_{13}H_{12}F_3NO$: C,61.17; H,4.74; F,22.33; N,5.49; O,6.27; Found: C,61.15; H,4.71; F, 22.35; N,5.48; O,6.31. LC/MS (ESI, *m/z)*: 255.1 $[M + H]^+$.

4-(3-(trifluoromethyl)phenyl)-5-vinylpyrrolidin-2-one (7g):

Pale white solid; yield 58%; m.p. 218–220 °C; UV(λ_{max}) 264.14 nm; IR spectra (KBr disc method, cm^{-1}): 1658.35, 938.10, 1156.60, 1389.46, 815.21, 594.11, 3395.26; ^{1}H NMR ($CDCl_3$, 500 MHz, δ_H): 4.125(s, 2H, –CH_2), 4.533 (d, $J = 10$ Hz, 2H, –CH linked to benzyl and –CH linked to vinyl) 5.186 (s, 2H, –CH_2 of vinyl), 5.449 (d, $J = 6$ Hz, 2H), 6.054(s, 2H), 7.399 (t, 1H), 7.537(t, 1H), 7.708 (d, $J = 8$ Hz, 1H), 7.966 (d, $J = 8.5$ Hz, 1H); ^{13}C NMR ($CDCl_3$, 125 MHz, δ_C): 166.888, 148.419, 147.921, 142.808, 138.102, 123.893, 119.063, 116.714, 106.592, 101.382, 57.738, 41.981, 33.304. Anal. $C_{13}H_{12}F_3NO$: C,61.17; H,4.74; F,22.33; N,5.49; O,6.27; Found: C,61.16; H,4.76; F, 22.36; N,5.43; O,6.29. LC/MS (ESI, *m/z)*: 254.9 $[M + H]^+$.

4-(3-hydroxyphenyl)-5-vinylpyrrolidin-2-one (7h):

Pale white solid; yield 60%; m.p. 149–151 °C; UV(λ_{max}) 252.70 nm; IR spectra (KBr disc method, cm^{-1}): 3331.18, 1627.97, 1577.82, 1226.77, 1155.40, 991.44, 783.13, 675.11; ^{1}H NMR ($CDCl_3$, 500 MHz, δ_H): 3.4775 (d, $J = 8.5$ Hz, 2H, $–CH_2$), 3.786 (s, 2H, –CH linked to benzyl and –CH linked to vinyl), 4.196 (dd, $J = 8.5$ Hz,16 Hz, 2H, $–CH_2$ of vinyl), 4.823 (s, 1H, –OH linked to benzyl), 5.416 (q, 1H, –CH of vinyl), 7.498–7.693 (m, 4H, aromatic region), 8.526 (s, 1H, –NH); ^{13}C NMR ($CDCl_3$, 125 MHz, δ_C): 179.977, 157.351, 143.852, 136.194, 130.029, 119.676, 119.440, 117.797, 115.075, 56.412, 40.137, 34.072. Anal. $C_{12}H_{13}NO_2$: C,70.92; H,6.45; N,6.89; O,15.74; Found: C,70.89; H,6.46; N,6.91; O,15.74. LC/MS (ESI, *m/z*): 203.11 $[M + H]^+$.

4-(3,4-dihydroxyphenyl)-5-vinylpyrrolidin-2-one (7i):

Pale white solid; yield 60%; m.p. 170–172 °C; UV(λ_{max}) 323 nm; IR spectra (KBr disc method, cm^{-1}): 1639.55, 1508.38, 669.32, 2534.55, 2654.14, 1959.74, 2789.16, 3639.31; ^{1}H NMR (DMSO-d_6, 500 MHz, δ_H): 4.520 (s, 2H, $–CH_2$), 4.810 (s, 2H, –OH groups), 4.962 (q, 1H, –CH of vinyl), 5.520 (s, 2H, –CH linked to benzyl and –CH linked to vinyl), 5.83 (dd, $J = 8.5$ Hz, 15 Hz, 2H, $–CH_2$ of vinyl), 6.521(s, 1H, –NH), 7.021 7.532 (m, 3H, aromatic region); ^{13}C NMR (DMSO-d_6, 125 MHz, δ_C): 167.746, 153.064, 144.056, 139.234, 129.874, 118.639, 105.748, 56.019, 30.683. Anal. $C_{12}H_{13}NO_2$: C,70.92; H,6.45; N,6.89; O,15.74; Found: C,70.93; H,6.42; N,6.92; O,15.73. LC/MS (ESI, *m/z*): 203.13 $[M + H]^+$.

4-(2-hydroxyphenyl)-5-vinylpyrrolidin-2-one (7j):

Pale white solid; yield 57%; m.p. 122–123 °C; UV(λ_{max}) 259.50 nm; IR spectra (KBr disc method, cm^{-1}): 1672.34, 1600.97, 748.41, 993.37, 1220.98, 1313.57, 698.25, 3354.32; ^{1}H NMR (DMSO-d_6, 500 MHz, δ_H): 4.273 (s, 2H, $–CH_2$), 4.683 (s, 2H, –CH linked to benzyl and -CH linked to vinyl), 5.361(dd, $J = 3$ Hz,11 Hz, 2H, $–CH_2$ of vinyl), 6.487 (s, 1H, -OH linked to benzyl), 6.520 (q, 1H, –CH of vinyl), 6.797–7.560 (m, $J = 15$ Hz, 4H, aromatic region), 9.077 (s, 1H, -NH); ^{13}C NMR (DMSO-d_6, 125 MHz, δ_C): 168.106, 156.671, 139.559, 131.355, 128.637, 120.892, 119.314, 118.281, 116.178, 57.738, 44.981, 30.692. Anal. $C_{12}H_{13}NO_2$: C,70.92; H,6.45; N,6.89; O,15.74; Found: C,71.00; H,6.41; N,6.93; O,15.66. LC/MS (ESI, *m/z*): 203.04 $[M + H]^+$.

4-(4-methoxyphenyl)-5-vinylpyrrolidin-2-one (7k):

Pale white solid; yield 45%; m.p. 150–152 °C; UV(λ_{max}) 253 nm; IR spectra (KBr disc method, cm^{-1}): 3331.18, 2926.11, 2850.88, 2364.81, 1627.97, 1541.18, 669.32; ^{1}H NMR ($CDCl_3$, 500 MHz, δ_H): 2.6275 (d, 2H, $–CH_2$), 2.946 (s, 2H, –CH linked to benzyl and –CH linked to vinyl), 3.189 (dd, $J = 7.5$ Hz,12 Hz, 2H, $–CH_2$ of vinyl), 4.1965 (s, 3H, $–OCH_3$), 4.987 (q, $J = 6$ Hz, 1H, –CH of vinyl), 6.4375 (s, 1H, –NH), 7.498–7.693 (m, 4H, aromatic region); ^{13}C NMR ($CDCl_3$, 125 MHz, δ_C): 180.077, 166.407, 157.033, 140.350, 133.708, 130.501, 129.322, 125.111, 123.088, 52.203, 49.277, 34.150. Anal. $C_{13}H_{15}NO_2$: C,71.87; H,6.96; N,6.45; O,14.73; Found: C,71.85; H,7.00; N,6.43; O,14.72. LC/MS (ESI, *m/z*): 217.09 $[M + H]^+$.

4-(3,4-dimethoxyphenyl)-5-vinylpyrrolidin-2-one (7l):

Pale white solid; yield 45%; m.p. 135–137 °C; UV(λ_{max}) 313 nm; IR spectra (KBr disc method, cm^{-1}): 1697.41, 1516.10, 684.75, 2519.12, 2519.12, 1876.80, 2960.83, 2841.24; ^{1}H NMR (DMSO-d_6, 500 MHz, δ_H): 6.44 (s, 1H, –NH), 3.787 (s, 6H, $–OCH_3$ groups), 4.54 (s, –CH linked to benzyl), 4.95(d, $J = 13.5$ Hz, 1H, –CH linked to vinyl), 5.520 (s, 2H, $–CH_2$), 5.83 (dd, $J = 8.5$ Hz,16 Hz, 2H, $–CH_2$ of vinyl), 6.96 (q, 1H, –CH of vinyl), 7.182–7.530 (m, 3H, aromatic region); ^{13}C NMR (DMSO-d_6, 125 MHz, δ_C): 167.919, 150.762, 148.974, 144.063, 127.090, 122.614, 116.824, 111.547, 110.319, 55.562-55.601, 40.007, 30.691. Anal. $C_{14}H_{17}NO_3$: C,68.00; H,6.93; N,5.66; O,19.41; Found: C,68.09; H,6.91; N,5.64; O,19.36. LC/MS (ESI, *m/z*): 249.1 $[M + H]^+$.

Estimation of GABA:

The GABase system (GABA-transaminase-succinic-semialdehyde dehydrogenase) had been utilized and has resulted in the formation of NADPH. The incubation mixture was consisting of a 0.1 M Tris-HCl buffer, pH 8.9, 3.2 mM α-Ketoglutarate, 0.5 mM NADP, 8 mM mercaptoethanol, GABase enzyme, and the tissue extract. After incubation for 50 min, fluorescence was observed on Shimadzu RF 1501 Spectrofluorophotometer at excitation and emission wavelength, 350 and 450 µm respectively [21]. A standard calibration curve of GABA was prepared, and the GABA was estimated in the tissue extract and was expressed as nmol/mg of protein. The Animals were sacrificed after 18 h and their brains were dissected. The frontal cortex was separated and was further homogenized and assayed for the estimation of change in the level of GABA.

In-vitro evaluation

GABA-AT inhibition assay

Different concentrations of the compounds were prepared in DMSO (100–1000 µM) and were incubated at 25 °C with 1 unit/ml of GABase prepared in buffer pH 7.2 (potassium phosphate buffer). Further, the reaction mixture was added consisting of 6 mM GABA in buffer pH 8.61 (potassium pyrophosphate buffer), 25 mM NADP+, 5 mM α-ketoglutaric acid, and 3.3 mM β-mercaptoethanol to the above mixture [22]. The procedure was repeated with the addition of the enzyme solution and the reaction mixture without the addition of the inhibitor. Blank was also prepared with the reaction mixture, a buffer of enzyme solution, and solvent

used in inhibitor preparation. The change in absorbance was measured by Biotek Synergy H1 multimode microplate reader. A calibration curve was made at a different concentration of compounds, and further IC_{50} values were calculated.

In-vitro kinetic study

Different concentrations of GABA (2–12 mM) were prepared in buffer, pH 8.6 (potassium pyrophosphate buffer), GABase 1 unit/ml in potassium phosphate buffer was incubated with reaction mixture (different GABA concentration (2–12 mM), 1.25 mM $NADP^+$, 5 mM α-ketoglutaric acid, and 3.3 mM β-mercaptoethanol) were added, and change in absorbance was measured. The same procedure was again repeated with the fixed concentration of inhibitor, and K_i was determined from the Lineweaver-Burk plot.

Hydrolysis study of the compound 7f in a simulated biological fluid

Hydrolysis study of the compound **7f** in a simulated biological fluid was studied in gastric (pH 1.2) and intestinal (pH 6.8) pH. An aliquot of 15 mL of this solution was withdrawn repeatedly and kept in test tubes maintained at 37 ± 0.5 °C. At a definite time interval (0.5 h, 1–8 h), an aliquot was withdrawn from different test tubes and was transferred to microcentrifuge tubes, followed by the addition of methanol to make up the volume. The tubes were placed in a freezing mixture to arrest further hydrolysis, followed by vortexing at high speed for 5 min. After vortexing, the tubes were centrifuged at high speed (3000 rpm) for 5 min. 5 mL of clear supernatant obtained from each tube was measured by a spectrophotometer for the amount of hydrolyzed compound released after the hydrolysis of compound **7f** in SGF and SIF at 230 nm [23]. The rate of hydrolysis of compound **7f** was computed as the percent of drug hydrolyzed based on the cumulative amount of drug hydrolyzed divided by the total amount of drug. The rate of hydrolysis and half-life of the compound **7f** was calculated according to the equations given below.

$$k = \frac{2.303}{t} \times \frac{a}{a - x} \quad (1)$$

$$t_{1/2} = \frac{0.693}{k} \quad (2)$$

where **k** is the rate constant, **t** is the time in hours; **a** is the initial concentration of conjugate, **x** is the amount of the compound hydrolyzed, a-x is the amount of compound remaining and $\mathbf{t_{½}}$ is the half-life of the compound [24].

In-vivo evaluation

All experimental studies were done following the laboratory animal care guidelines (NIH publication no.85-23 revised 1985) and were also approved by the Institutional Animal Ethical Committee, Banaras Hindu University (BHU; Dean/2016/CAEC/1651). The subjected Sprague–Dawley rats, weighing 150–200 gms, were purchased from Central Animal House, Institute of Medical Science (IMS-BHU). They were kept and maintained in the animal house under a controlled environment (Temperature 25 ± 1 °C) RH 45–55%), food and water ad libitum, and a 12:12 h light/dark cycle. Before conducting the experiments, animals were kept at an acclimatization period of at least one week in the experimental lab.

Maximal Electroshock Induced Seizures test (MES) model

The Sprague–Dawley rats (male & female), of weight 150–200 g (adult male) administered orally by gavage (volume of 0.5 ml) the standard drug and the synthesized compounds. The 100 mg/kg dose was taken for the standard, and three doses of 50, 100, and 200 mg/kg were selected for the test compounds. The DMSO solution and no drug were given to the control and diseased group comparatively control group received DMSO solution orally, whereas the diseased group received no drug. After 1 h of drug administration, an electrical stimulus (50 mA at 60 Hz) was transmitted across the brain in 0.2 s via a pair of clip electrodes to induce a seizure [25]. After applying the shock, the animals were then observed for the type of convulsions produced, and the endpoint of the seizure produced was determined by the tonic hind limb extension and was taken in three phases tonic, clonic, and stupor phases. The protection against seizure was considered a reduction in time or total absence in hind limb tonic extension [26].

Pentylenetetrazole (PTZ)-Induced Seizures test

All the animals were checked to rule out any infection or illness. The dose used in the study were Pentylenetetrazole (90 mg/kg) Vigabatrin (100 mg/kg), and Test compounds (50, 100, 200 mg/kg). Total rats were divided randomly into six groups, each group containing six rats. The designed groups were assigned in to Control (DMSO solution), Diseased (No drug), Standard (Vigabatrin 100 mg/kg), Test (t1) (50 mg/kg), Test (t2) (100 mg/kg) and Test (t3) (200 mg/kg). The drugs were administered to animals orally by gavage under appropriate precautions as per the study group. After sixty minutes, the PTZ solution was administered by s.c. route under aseptic precautions. The occurrence of the seizure in animals was observed for 30 min

[21]. The occurrence of the seizures which was considered a positive seizure response (clonic seizure for more than five seconds), protection against the PTZ seizures (abolition of the clonic seizure) was determined. The different parameters, seizure latency (interval between PTZ injection and onset of seizure activity) in Sec. and clonic phase of the seizure (time duration in sec.) were studied for the seizure occurrence. After thirty minutes the animals were inspected for any injury or residual damage [27].

Histopathological examination of PTZ treated Rat Brains

After treatment with PTZ solution and compound **7f**, the rat was sacrificed by the decapitation technique. The hippocampus was isolated from the rat brain by surgery. The hippocampal part was embedded into 10% formalin for microtoming of tissues and preparation of thin slices of hippocampal neurons. The thin slices of the hippocampus were treated with dyeCresyl-Fast (violet stain) for Nissl staining (highlight neuron structural features) and then observed under a photomicroscope for any tissue damage as well as morphological changes.

Biochemical assay of GABA in the cortical region

Sprague–Dawley male and female rats, bodyweight 150–200 gm, were subjected to anesthetized with sodium pentobarbital injection (35 mg/kg; i.p.), then fixed on the stereotaxic frame which holds the scalp of the anesthetized rat was incised and retracted with a needle, bregma was positioned in the scalp of anesthetized rats. All coordinates were set from the bregma (0,0) point and drilled +3.5 mm anteroposterior, mediolateral ± 0.6 mm, and −5.2 mm dorsoventral from the bregma point [28]. The compound **7f** (5, 10, and 20 µg/µl) and the standard drug (Vigabatrin) (10 µg/µl) were administered to the rats by intracerebroventricular (ICV) route in a volume of 0.1 µl at the infusion rate of 0.2 µl/min [29]. The control group received no drug whereas the sham group (placebo surgery group) received saline solution intracerebrally. The transmission of an electrical stimulus (50 mA at 60 Hz) of 0.2 sec in duration via a pair of clip electrodes and an across the brain was used to induce the seizure after 18 hr of the drug administration [30]. After applying the shock, the animals were then observed for the type of convulsions produced, and the endpoint of the seizure produced was determined by the tonic hind limb extension and was taken in three phases tonic, clonic, and stupor phases. The protection against seizure was considered a reduction in time or total absence in hind limb tonic extension. The animals were killed (by decapitation) after the behavioral studies conducted [31]. The dissected Frontal cortex (from each animal) was stored at −80 °C for further use.

The extraction was carried out by mixing followed by homogenization (using glass homogenizer) of the tissue sample, 10 vol. of cold 0.5 M perchloric acid with 1 mM EDTA (ethylenediaminetetraacetic acid), and the mixed volume was centrifuged for 15 min at 4500 rev/min. Further, the supernatant was neutralized with $KHCO_3$ and subjected to centrifuge again; thus the supernatant obtained was collected and stored at −80 °C for further use. The pellet was suspended in 0.1 N NaOH, and protein concentration was measured by the Lowry et al. method.

In-silico studies

The Docking studies were performed using the Glide module of Schrödinger 2018-1. The docking validation of vigabatrin (co-crystallized ligand, standard) was carried out by using the superposition protocol. The 2D sketch tool was used to draw the compounds, and the LigPrep tool was used for generating the low-energy conformers of the designed ligands using force field OPLS-2005 [32]. The generated conformers were further used for molecular docking studies. The 3D crystallographic structure of GABA-AT complexed with Vigabatrin (RCSB, Protein Data Bank, PDB ID: 1OHW) was used for computational docking studies [33]. The protein preparation and error correction was accomplished by the protein preparation wizard module. The grid was created by use of the receptor grid generation module of glide, retaining the default settings, over the active site considering the ligand. The validation of the Grid is done by re-docking of the Vigabatrin (co-crystallized ligand) in generated Grid, and the docking protocol was confirmed by the interaction of the docked pose (amino acid residues of the active site with Vigabatrine) with co-crystallized ligands were in agreement with the reported literature. The extra precision (XP) mode was used for the calculations of the lowest energy conformers of ligands by keeping other parameters of the Glide module at their default values. The interaction of the ligand molecules (hydrophobic, hydrogen bond interactions) with the active site pocket (participating amino acids) of GABA-AT was also determined. The computational study was initiated and resulted in docking scores of the synthesized compounds and Vigabatrin.

Molecular dynamics simulations

A molecular dynamics simulation study was used to predict the stability and conformational changes of the compound in the protein active site. The optimized dock conformation of the most active compound **7f** was introduced in the Desmond module of Schrödinger for MD simulation studies. Using the system builder module, the orthorhombic simulation box was prepared around the docked complex. The TI3P explicit water model was used to mimic the real environment of humans

[34]. Further, the whole system was neutralized by the addition of 3 Na^+ counter ions, and 0.15 M NaCl was added to provide the isosmotic salt environment. Further, we performed a relaxation model system before the simulation run. The soaked simulation system was later subjected to dynamics simulation of 50 ns using OPLS 2005 force field. The recording interval was kept at 1.2 ps, and the trajectory was set at 9.6. The simulation runs were performed at a constant number of the atom (N), pressure (P), and temperature (T) (NPT) ensemble. The temperature and pressure were kept at 300 K and 1.013 bars of atmospheric pressure during the simulation runs. The built-in module simulation interaction analysis was further used for analyzing the trajectories obtained after the MD simulation studies.

MMGB-SA and ADME prediction

The MMGB-SA and drug-likeliness characteristics were predicted using the Superposition and QikProp module of Schrodinger Maestro 2018-1, respectively. Several descriptors were predicted such as SASA, Mol log P, and pKa of most Basic/Acidic groups to evaluate the drug-likeliness property in the compound as per the Lipinski's rule of five (mol_MW < 500, QPlogPo/w < 5, donorHB ≤5, accptHB ≤10).

Acknowledgements The authors of the presented work would like to gratefully acknowledge the Indian Institute of Technology (Banaras Hindu University), Varanasi, for providing financial and necessary infrastructural facilities to carry out the experiments. The author Digambar K. Waiker would like to thank CSIR for providing financial support (CSIR-SRF File. No. 09/1217(0046)/2017 EMR-1).

Compliance with ethical standards

Conflict of interest The present work is an original idea of the authors and carried out with the support of the Indian Institute of Technology Banaras Hindu University, Varanasi. The authors of the present work also declare no conflict of interest.

Publisher's note Springer Nature remains neutral with regard to jurisdictional claims in published maps and institutional affiliations.

References

1. Seth A, et al. Design, synthesis, evaluation and molecular modeling studies of some novel N-substituted piperidine-3-carboxylic acid derivatives as potential anticonvulsants. Medicinal Chem Res. 2018;27:1206–25.
2. Wu C, Sun D. GABA receptors in brain development, function, and injury. Metab brain Dis. 2015;30:367–79.
3. Sahu M, et al. Design, synthesis and evaluation of newer 5, 6-dihydropyrimidine-2 (1H)-thiones as GABA-AT inhibitors for anticonvulsant potential. Bioorg Chem. 2017;74:166–78.
4. Yoon B-E, Lee CJ. GABA as a rising gliotransmitter. Front neural circuits. 2014;8:141.
5. Ben-Ari Y. Seizures beget seizures: the quest for GABA as a key player. Crit Rev Neurobiol. 2006;18:1–2.
6. Błaszczyk JW. Parkinson's disease and neurodegeneration: GABA-collapse hypothesis. Front Neurosci. 2016;10:269.
7. Solas M, Puerta E, Ramirez MJ. Treatment options in alzheimer s disease: the GABA story. Curr Pharm Des. 2015;21:4960–71.
8. Treiman DM. GABAergic mechanisms in epilepsy. Epilepsia. 2001;42:8–12.
9. Pehrson AL, et al. The influence of NMDA and GABA A receptors and glutamic acid decarboxylase (GAD) activity on attention. Psychopharmacology. 2013;225:31–39.
10. Das N, Dhanawat M, Shrivastava SK. An overview on antiepileptic drugs. Drug discov ther. 2012;6:178–93.
11. Schechter PJ, Vigabatrin. In The Medical Treatment of Epilepsy. 2020, CRC Press. p. 313–8.
12. TASHEVA D, et al. Reactions of glycine schiff base derivatives and cinnamates under aqueous conditions. Preparation ß-Phenylglutamic Acid Derivatives. 2005;97:123.
13. Hassib HB, Abdel-Kader NS, Issa YM. Kinetic study of the hydrolysis of schiff bases derived from 2-aminothiophenol. J Solut Chem. 2012;41:2036–46.
14. Shah K, Shrivastava SK, Mishra P. Evaluation of mefenamic acid mutual prodrugs. Medicinal Chem Res. 2013;22:70–77.
15. Huang LT, et al. Pentylenetetrazol-induced recurrent seizures in rat pups: time course on spatial learning and long-term effects. Epilepsia. 2002;43:567–73.
16. Choi S, et al. Design of a conformationally restricted analogue of the antiepilepsy drug vigabatrin that directs its mechanism of inactivation of γ-aminobutyric acid aminotransferase. J Am Chem Soc. 2002;124:1620–4.
17. Das N, et al. Design, synthesis, preliminary pharmacological evaluation, and docking studies of pyrazoline derivatives. Chem Pap. 2012;66:67–74.
18. Paschke A, et al. Octanol/water partition coefficient of selected herbicides: determination using shake-flask method and reversed-phase high-performance liquid chromatography. J Chem Eng Data. 2004;49:1639–42.
19. Dekeukeleire S. et al. Rhodium-catalysed hydroformylation of N-(2-propenyl)-β-lactams as a key step in the synthesis of functionalised N-[4-(2-oxoazetidin-1-yl) but-1-enyl] acetamides. N J Chem. 2010;34:1079–83.
20. Dryanska V, Pashkuleva I. A simple and efficient synthesis of γ-aminobutyric acid (GABA) derivatives. Org preparations Proced Int. 1999;31:232–6.
21. Das N, et al. Synthesis and pharmacological evaluation of some N 3-aryl/heteroaryl-substituted 2-(2-chlorostyryl)-6, 7-dimethoxyquinazolin-4 (3 H)-ones as potential anticonvulsant agents. Medicinal Chem Res. 2014;23:4167–76.
22. Juncosa JI Jr, et al. Probing the steric requirements of the γ-aminobutyric acid aminotransferase active site with fluorinated analogues of vigabatrin. Bioorg medicinal Chem. 2013;21:903–11.
23. Rasheed A, Kumar C. Design, synthesis, hydrolysis kinetics and phamacodynamic profiles of histidine and alanine conjugates of aceclofenac. Acta Pharmaceutica. 2010;60:99.
24. Shrivastava SK, et al. Flurbiprofen-and suprofen-dextran conjugates: synthesis, characterization and biological evaluation. Trop J of Pharm Res. 2009;8:3.
25. Dhanawat M, Banerjee AG, Shrivastava S. Design, synthesis, and anticonvulsant screening of some substituted piperazine and aniline

derivatives of 5-phenyl-oxazolidin-2, 4-diones and 5, 5-diphenylimidazolidin-2, 4 diones. Medicinal Chem Res. 2012;21:2807–22.
26. Sahu M, et al. 5, 6-Dihydropyrimidine-1 (2H)-carbothioamides: Synthesis, in vitro GABA-AT screening, anticonvulsant activity and molecular modelling study. Bioorg Chem. 2018;77:56–67.
27. Swinyard E. General principles. Experimental selection, quantification, and evaluation of anticonvulsants. Antiepileptic drugs. 1989:85–102.
28. Birrell JM, Brown VJ. Medial frontal cortex mediates perceptual attentional set shifting in the rat. J Neurosci. 2000;20:4320–4.
29. Iadarola MJ, Gale K. Substantia nigra: site of anticonvulsant activity mediated by gamma-aminobutyric acid. Science. 1982;218:1237–40.
30. Neal M, Shah M. Development of tolerance to the effects of vigabatrin (γ-vinyl-GABA) on GABA release from rat cerebral cortex, spinal cord and retina. Br J Pharmacol. 1990;100:324–8.
31. Rijn CMV, et al. Decapitation in rats: latency to unconsciousness and the 'wave of death'. PloS one. 2011;6:e16514.
32. Tripathi PN, et al. Design and development of novel N-(pyrimidin-2-yl)-1, 3, 4-oxadiazole hybrids to treat cognitive dysfunctions. Bioorg medicinal Chem. 2019;27:1327–40.
33. Storici P. et al. Structures of γ-aminobutyric acid (GABA) aminotransferase, a pyridoxal 5′-phosphate, and [2Fe-2S] cluster-containing enzyme, complexed with γ-ethynyl-GABA and with the antiepilepsy drug vigabatrin. J of Biol Chem. 2004;279:363–73.
34. Sinha SK, Shrivastava SK. Synthesis, evaluation and molecular dynamics study of some new 4-aminopyridine semicarbazones as an antiamnesic and cognition enhancing agents. Bioorg med Chem. 2013;21:5451–60.